RESEARCH ARTICLE

National Science Review
6: 524–531, 2019
doi: 10.1093/nsr/nwz010
Advance access publication 22 January 2019

PHYSICS

Stoichiometric evolutions of PH_3 under high pressure: implication for high-T_c superconducting hydrides

Ye Yuan[1,†], Yinwei Li[2,†], Guoyong Fang[3,†], Guangtao Liu[1], Cuiying Pei[1], Xin Li[1,4], Haiyan Zheng[1], Ke Yang[5] and Lin Wang[1,*]

ABSTRACT

The superconductivity of hydrides under high pressure has attracted a great deal of attention since the recent observation of the superconducting transition at 203 K in strongly compressed H_2S. It has been realized that the stoichiometry of hydrides might change under high pressure, which is crucial in understanding the superconducting mechanism. In this study, PH_3 was studied to understand its superconducting transition and stoichiometry under high pressure using Raman, IR and X-ray diffraction measurements, as well as theoretical calculations. PH_3 is stable below 11.7 GPa and then it starts to dehydrogenate through two dimerization processes at room temperature and pressures up to 25 GPa. Two resulting phosphorus hydrides, P_2H_4 and P_4H_6, were verified experimentally and can be recovered to ambient pressure. Under further compression above 35 GPa, the P_4H_6 directly decomposed into elemental phosphorus. Low temperature can greatly hinder polymerization/decomposition under high pressure and retains P_4H_6 up to at least 205 GPa. The superconductivity transition temperature of P_4H_6 is predicted to be 67 K at 200 GPa, which agrees with the reported result, suggesting that it might be responsible for superconductivity at higher pressures. Our results clearly show that P_2H_4 and P_4H_6 are the only stable P–H compounds between PH_3 and elemental phosphorus, which is helpful for shedding light on the superconducting mechanism.

Keywords: high pressure, hydrides, superconductivity, stoichiometric evolution

[1]Center for High Pressure Science and Technology Advanced Research, Shanghai 201203, China; [2]School of Physics and Electronic Engineering, Jiangsu Normal University, Xuzhou 221116, China; [3]Key Laboratory of Carbon Materials of Zhejiang Province, College of Chemistry and Materials Engineering, Wenzhou University, Wenzhou 325035, China; [4]Department of Physics, Fudan University, Shanghai 200433, China and [5]Shanghai Institute of Applied Physics, Chinese Academy of Sciences, Shanghai 201203, China

*Corresponding author. E-mail: wanglin@hpstar.ac.cn
†Equally contributed to this work.

Received 9 November 2018; **Revised** 9 December 2018; **Accepted** 21 January 2019

INTRODUCTION

Since superconducting mercury was first reported [1,2], scientists have continued to search for new high critical temperature (T_c) materials. In 2004, Ashcroft studied hydrogen-dominant hydrides [3], in which condensed H_2 may contribute to a high T_c. Motivated by this work, extensive theoretical investigations on this system have been reported, such as SiH_4 [4], GeH_4 [5], GaH_3 [6], $SiH_4(H_2)_2$ [7], CaH_6 [8] and YH_6 [9], etc. A few remarkable high-T_c materials have also been observed in subsequent experimental studies. Recently, Drozdov *et al.* reported the superconductive transition of H_2S at 203 K and 155 GPa [10], which broke the highest T_c record [11]. Many theoretical [12,13] and experimental [14] studies have explored its stoichiometry and structure, which play an important role in understanding the underlying mechanism of superconductivity.

Very recently, PH_3, a typical hydrogen-rich hydride, has attracted a great deal of research interest because of its superconducting transition discovered by Drozdov and his co-workers [15–20]. Their experimental work revealed that PH_3 might be a high-temperature superconducting candidate. From the resistance measurements, a superconducting transition signature was observed at T_c of 30 K. This increased to 103 K with pressures up to 207 GPa. However, structural information was not provided, and the origin of the superconducting transition remains puzzling. Subsequent theoretical studies [16–19] showed that the P–H compound should also be a complex system, and all the predicted structures were metastable with respect to the elemental phase.

Flores-Livas *et al.* [16] studied the phase diagram of phosphorus hydrides with different stoichiometries and found that they tended to decompose into phosphorus and hydrogen at high pressure.

Liu *et al.* [17] predicted a PH_3 phase with a monoclinic structure (C2/m) and a T_c of 83 K at 200 GPa, which is closer to the observed superconducting transition temperature. Shamp *et al.* [18] predicted that PH_3 is thermodynamically unstable during decomposition into the elemental phases, as well as PH_2 and H_2. Two PH_2 phases with C2/m and I4/mmm symmetry were computed as metastable at 200 GPa. The corresponding superconducting critical temperatures were 76 and 70 K, respectively. Bi *et al.* [19] found that a dynamically stable PH_2 phase was the best according to the observed superconducting transition at 80 GPa. The PH_3 phase to PH_2 phase reaction was exothermic at that pressure, which proves the spontaneity of the reaction.

Until now, the PH_3 phase under compression has remained unknown and no relevant experimental studies have been reported. The high-pressure stoichiometry and structural behavior of PH_3 are critical to understanding the superconducting transition in the P–H system, which needs to be experimentally determined. For this purpose, we studied the structural behavior of PH_3 under high pressure. We identified the pressure-induced step-by-step polymerization of PH_3 and a route to elemental phosphorus that unveiled the unknown transition process and provides experimental evidence for understanding the underlying mechanism of the superconductivity of P–H compounds.

RESULTS AND DISCUSSION

Stoichiometric evolutions of PH_3 at room temperature

After the PH_3 gas was loaded into the sample chamber of the diamond anvil cell (DAC) and returned to room temperature, a colorless and transparent sample (Supplementary Fig. 1, available as Supplementary Data at *NSR* online) was observed. The characteristic Raman peaks (Supplementary Fig. 1, available as Supplementary Data at *NSR* online) at 978 (υ_2, symmetric bending mode), 1104 (υ_4, asymmetric bending mode), 2317 (υ_1, stretching mode) and 2331 (υ_3, stretching mode; shoulder) cm^{-1} agreed well with previous reports [21], indicating the existence of PH_3 in the chamber.

The X-rays can damage the sample (Supplementary Fig. 2, available as Supplementary Data at *NSR* online), so Raman and infrared absorption spectroscopy (IR) were mainly used for our *in situ* studies of PH_3 at high pressure. Figure 1a and c shows the Raman spectra of the sample during compression. Under high pressure, these characteristic modes blue shifted and broadened (Fig. 1b and d) and eventually vanished at 20.5 GPa. Several new peaks (marked by black asterisks and arrows in Fig. 1a) were observed at around 11.7 GPa, which suggested a phase transition. For the P–H stretching modes, we also noticed a dramatic expansion of the characteristic bonds. Figure 1d shows the peak positions of the υ_1 and υ_3 modes as a function of pressure. The peak shift of υ_1 dramatically decreased and started to red shift at 11.7 GPa. We attributed these changes to a transition in the sample near 11.7 GPa.

These new peaks in the Raman spectra (Fig. 1a) were consistent with previous studies about P_2H_4 at ambient pressure. The two new peaks at low frequencies correspond to the PH_2 rocking mode and P–P stretching mode in the P_2H_4 molecule, which were observed at around 217 and 436 cm^{-1}, respectively [22,23]. The emergency P–P bond at 11.7 GPa proved the dimerization of PH_3 molecules. The other new peaks at 1007 and 1093 cm^{-1} were from the PH_2 scissoring modes in the P_2H_4 molecule, which also agrees with previous reports. These factors suggest that the pressure-induced transition is due to the dimerization of PH_3 at high pressure.

To verify the dimerization, we also studied the decompressed sample. A liquid sample was obtained after quenching to ambient conditions, as shown in the microphotograph of the decompressed sample (inset optical images in Fig. 2a). It is well known that P_2H_4 is a liquid at ambient pressure [22,24], which confirms that pressure drives the dimerization of PH_3 to form P_2H_4 via this reaction:

$$2PH_3 \rightarrow P_2H_4 + H_2. \quad (1)$$

We further employed Raman to measure the recovered liquid sample. However, after laser irradiation, the liquid sample decomposed and generated Hittorf's phosphorus [25,26] (Fig. 2a) according to the photodecomposition properties of P_2H_4 [24]. This offers more evidence of our findings.

We also employed IR to trace the *in situ* information of the new product at high pressure. Supplementary Fig. 3a, available as Supplementary Data at *NSR* online, shows the IR peak near 1095 cm^{-1} broadened and shifted slightly to a lower frequency with increasing pressure, but an obvious new shoulder was observed at around 1058 cm^{-1} after decompressing the sample to 11.8 GPa (Supplementary Fig. 3c and d, available as Supplementary Data at *NSR* online). This new shoulder matched the P_2H_4 scissors mode well, which was observed at around 1052 cm^{-1} in a solid state at ambient pressure [27]. This characteristic mode confirms the existence of P_2H_4. In addition to the P–H stretching modes in the IR spectra (Supplementary Fig. 3b, available as

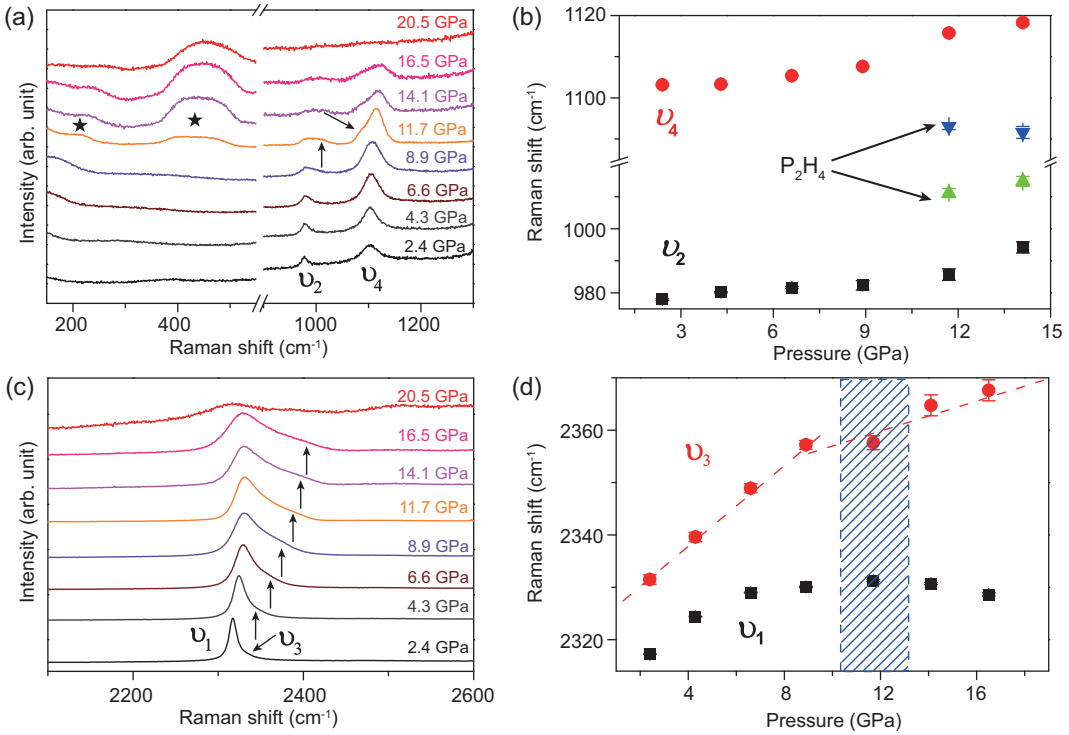

Figure 1. (a, c) Raman spectra of PH_3 at various pressures at room temperature. The peak positions of υ_2, υ_4 (b) and υ_1, υ_3 (d) as functions of pressure.

Supplementary Data at *NSR* online), a new shoulder at around 2329 cm^{-1} was observed, and it became stronger and stronger with increasing pressure. After it had quenched to 11.8 GPa, the new shoulder peak was more obvious compared to the IR spectrum measured at 12 GPa during compression. This proves dimerization.

As the pressure increased, the P_2H_4 showed piezochromism. It became yellow, then red and darkened, and eventually became opaque at pressures higher than 25 GPa, consistently with the observations of Drozdov *et al.* at low temperatures (180 K). As the sample became totally opaque, the vibrational signal vanished and hindered the *in situ* high-pressure vibrational spectra measurement. Therefore, we had to quench the sample to ambient conditions from different pressures (25 and 35 GPa) and employed Raman spectroscopy to investigate the different quenched residues. Interestingly, once the sample became completely opaque above 25 GPa, it maintained its opaque solid state even when decompressed to room pressure. This irreversible process suggests that a new transition occurred at higher pressures.

Figure 2b shows that the Raman spectrum of the residue quenched from 25 GPa after the opaque transition. A weak peak near 873 cm^{-1} belonging to PH_2 twisting and a strong peak at 2248.5 cm^{-1} belonging to P–H stretching exist in the spectrum. This new P–H stretching peak is located at a much lower wave number than in PH_3, P_2H_4 (~2292 cm^{-1}) and P_3H_5 (~2267 cm^{-1}) [24], suggesting that the residue contained a new kind of phosphorus hydride. Figure 2c shows the P–H stretching mode of P_nH_{n+2} shifts to lower frequency as n becomes larger. Following this trend, we deduced that the new phosphorus hydride was P_4H_6, which suggests that the P_2H_4 molecules continued to dimerize and form P_4H_6 at higher pressure.

To confirm the second dimerization, we calculated the Raman modes of P_4H_6 using the Gaussian 09 program at the B3LYP/6–311(d, p) level [28]. Supplementary Table 1, available as Supplementary Data at *NSR* online, shows the calculated Raman modes of two typical P_4H_6 conformers, in which the four phosphorus atoms are linear and U-type (Supplementary Fig. 4a and b, available as Supplementary Data at *NSR* online). The calculated Raman spectra show that they both have four characteristic bands corresponding to the stretching vibration (350–450 cm^{-1}) of the P–P bond, twisting vibration (700–900 cm^{-1}) of the PH_2 group, scissoring vibration (~1070 cm^{-1}) of the PH_2 group and stretching vibration of the P–H bond, respectively. Moreover, the P–H stretching mode can further shift to a lower frequency (2278 cm^{-1}).

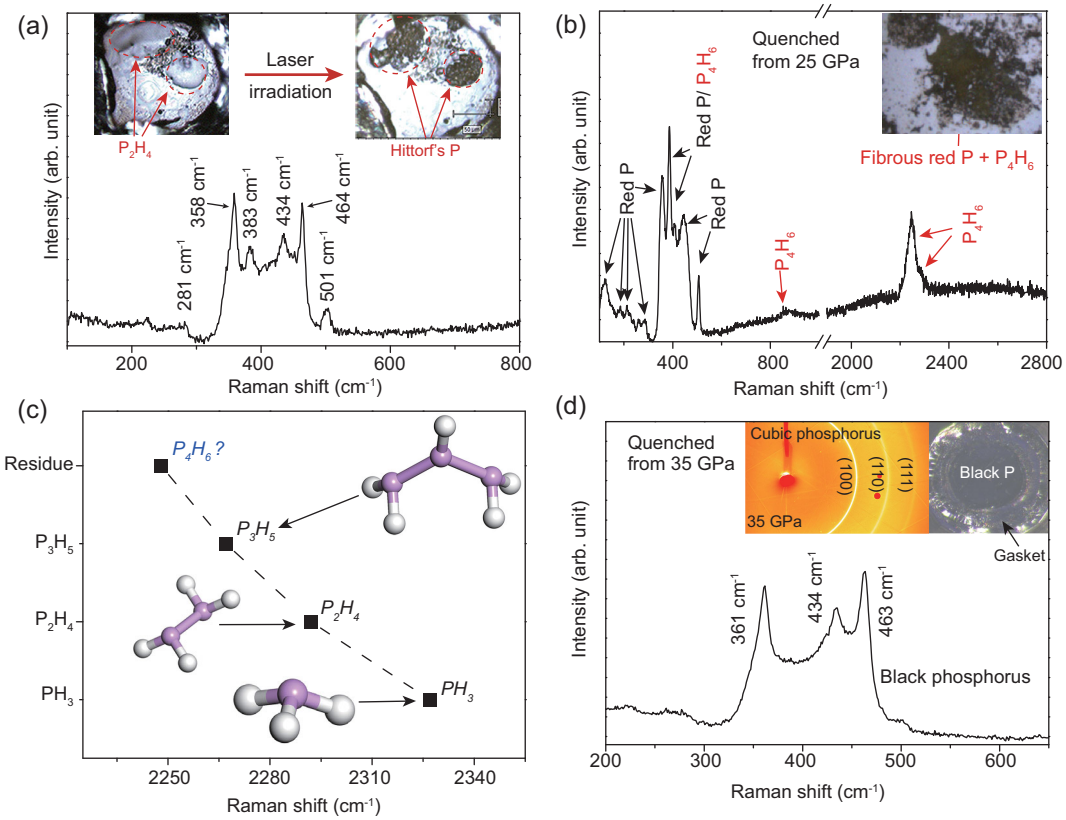

Figure 2. (a) The Raman spectrum of the Hittorf's phosphorus transformed from the liquid sample after laser irradiation. The inset images show the photo-induced transition of the liquid residue before and after laser irradiation. (b) The Raman spectrum of the sample decompressed from 25 GPa. The inset picture shows the optical micrograph of the decompressed sample. (c) The frequency trend of the P–H stretching in P_nH_{n+2} ($n = 1, 2, 3$ and 4). (d) The Raman spectrum of the sample quenched from 35 GPa. The inset shows the XRD pattern of the sample at 35 GPa and the optical micrograph of the decompressed sample.

From Supplementary Table 1, available as Supplementary Data at *NSR* online, we can see that the P–P stretching bonds and the twisting vibration of the PH_2 group from linear P_4H_6 are closer to our observed peak, suggesting that the linear type P_4H_6 is the more possible conformer in the residue.

Besides the peaks from P_4H_6, several other obvious characteristic modes (123.8, 184.8, 218.9, 285, 357.2, 386.5, 407.7, 443.2 and 505.8 cm^{-1}) were observed below 550 cm^{-1}. These peaks are similar to fibrous red phosphorus characteristic modes [25,26], which indicated that parts of P_4H_6 were thoroughly dissociated when exposed to laser or decompression. At ambient pressure, phosphorus hydrides often undergo disproportionation into phosphorus-rich phosphanes upon exposure to light and heat [24]. However, we did not observe the Raman peaks from other phosphanes from the residue, which proves that P_2H_4 dimerized directly into P_4H_6 at high pressure, corresponding to this equation:

$$2P_2H_4 \rightarrow P_4H_6 + H_2. \quad (2)$$

From the recovered sample, it is confirmed that P_2H_4 dimerizes at high pressure. However, as both Raman and IR signal disappeared at above 20 GPa, we could not get *in situ* high-pressure vibrational modes. Therefore, it might be possible that other compounds generated at high pressure, such as $P_4H_6{\cdot}H_2$, which may easily decompose back to P_4H_6 and H_2 upon decompression.

Figure 2d shows that the Raman spectra of the residue quenched from 35 GPa. After decompression to 1 atm, typical black phosphorus modes were observed [29,30]. Therefore, P_4H_6 eventually decomposed into elemental phosphorus at 35 GPa. Hence, the corresponding reaction is as follows:

$$P_4H_6 \rightarrow 4P + 3H_2. \quad (3)$$

From the *in situ* high-pressure XRD (Fig. 2d), the typical diffraction rings of cubic phosphorus further confirmed the thorough decomposition of P_4H_6 at high pressure.

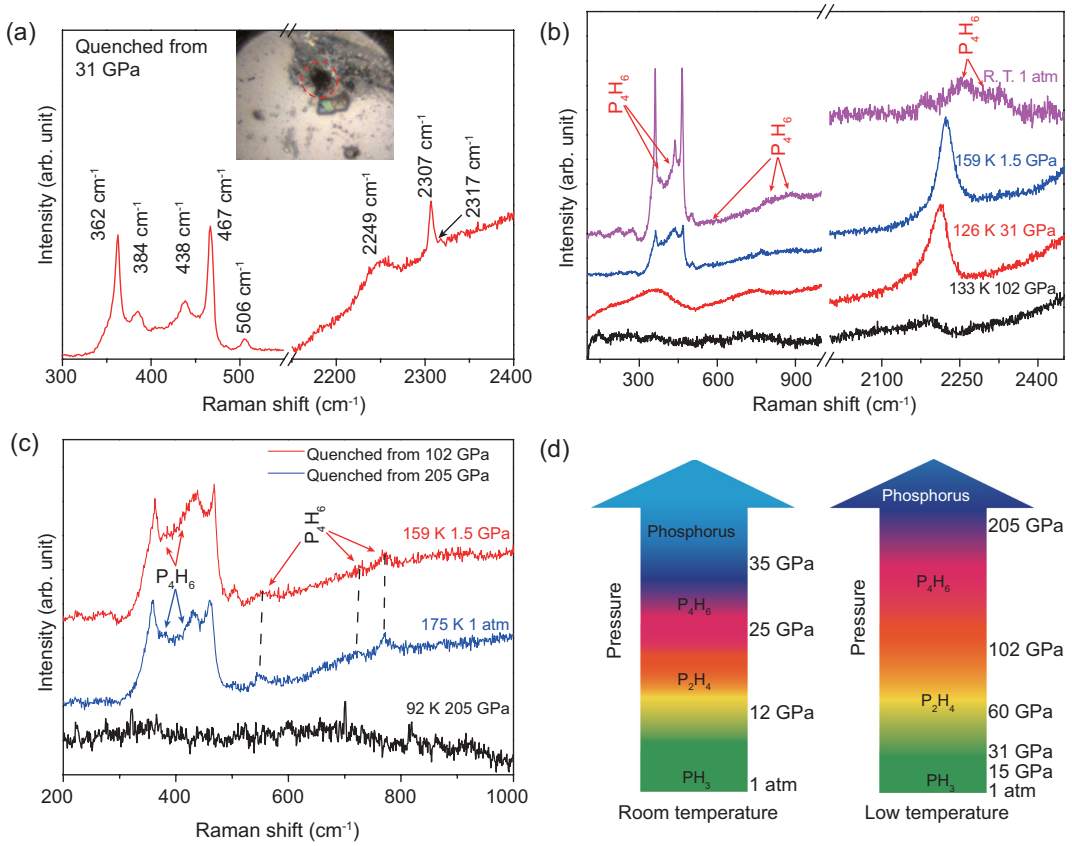

Figure 3. (a) The Raman spectrum of the sample quenched from 31 GPa. The inset image shows the photo-induced transition after laser irradiation. (b) The Raman spectra of the sample collected during decompression from 102 GPa. (c) The Raman spectra of the residue quenched from 205 (blue line) and 102 (red line) GPa, respectively. (d) The phase diagrams of PH_3 at room temperature and low temperature.

Stoichiometric evolutions of PH_3 at low temperature

The superconductivity of elemental phosphorus has already been studied both experimentally and theoretically [31–33]. The maximum T_c is about 9.5 K at 32 GPa before it decreases with pressure. Near 100 GPa, the T_c is about 4.3 K at 160 GPa, and no superconducting transition was detected in the temperature range from 4 to 40 K. The much lower T_c of phosphorus compared to 100 K indicates that PH_3 or other phosphorus hydrides should be responsible for the superconductivity observed at 200 GPa in Drozdov's work. Since Drozdov *et al.* increased the pressure at low temperature (T <200 K) [15], we speculate that this discrepancy is due to the different experimental protocols used in these two works. Low temperature could hinder the polymerization/decomposition of phosphorus hydrides and secure phosphorus hydrides to much higher pressure.

To find out whether low temperature can hinder the reactions and further indentify the superconducting candidate, we studied the high-pressure behavior of PH_3 at low temperature (<200 K). First, we compressed PH_3 up to 31 GPa, when P_2H_4 dimerized into P_4H_6 at room temperature. However, after we decompressed the sample to ambient pressure at low temperature, the sample became transparent again (the inset image in Fig. 3a). As shown in Fig. 3a, the sample decomposed after laser irradiation and the resulting opaque solid (the inset image in Fig. 3a was identified as Hittorf's phosphorus) and two characteristic Raman modes from P_2H_4 (2307 and 2317 cm^{-1}) were also found. The transparency of the residue and strong peaks from P_2H_4 suggest P_2H_4 was dominant in the sample decompressed from 31 GPa at low temperature. However, it can only survive below 25 GPa at room temperature, proving that low temperature can greatly hinder the polymerization of phosphorus hydrides. We further compressed the sample up to 60 GPa, and studied the Raman spectrum of the quenched residue. Similar photodecomposition and typical Hittorf's P Raman modes (Supplementary Fig. 5, available as Supplementary Data at *NSR*

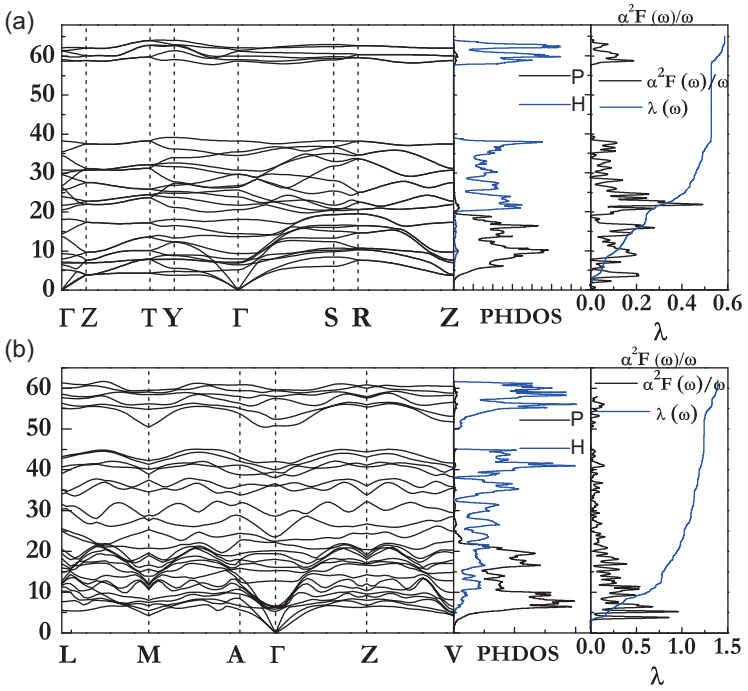

Figure 4. Phonon dispersions, phonon density of states projected onto atoms (PHDOS), the spectral functions $\alpha^2F(\omega)/\omega$ and electron–phonon coupling integration of $\lambda(\omega)$ for the (a) Cmcm structure at 100 GPa and (b) C2/m structure at 200 GPa, respectively.

online) were observed, which further suggested that P_2H_4 could remain up to 60 GPa at low temperature.

As the superconductivity was observed at pressures >80 GPa, we compressed PH_3 at low temperature up to 102 and 205 GPa, respectively, to investigate the responsible superconducting candidate. As shown in Fig. 3b and c, we did not observe any peaks from the Raman spectra at 102 and 205 GPa, due to its metallic state as identified by Drozdov *et al.* After decompressing to 31 GPa, a strong peak at around 2212 cm^{-1} was observed, and it shifted to around 2250 cm^{-1} after the sample was quenched to ambient conditions. We also observed several other peaks at around 383, 418, 798 and 880 cm^{-1}, which agreed well with our simulated P_4H_6 (Supplementary Table 1, available as Supplementary Data at *NSR* online) Raman, confirming the residue recovered from 102 GPa and 133 K was P_4H_6. As shown in Fig. 3c, the Raman spectrum of the sample decompressed from 205 GPa is almost the same as that from 102 GPa, suggesting P_4H_6 could be stable up to 205 GPa at low temperature. As P_4H_6 was observed after decompression from 102 and 205 GPa, we propose that the corresponding superconducting candidate in Drozdov's work could be P_4H_6. By combining the PH_3 structure evolutions at both room and low temperatures, we could obtain the phase diagram of PH_3 under high pressure (Fig. 3d).

Table 1. The calculated electron–phonon coupling constants (λ), the logarithmic average phonon frequency (ω_{log}) and the T_c with $\mu^* = 0.13$.

Phases	Pressure (GPa)	λ	ω_{log}	T_c ($\mu^* = 0.13$)
Cmcm	100	0.59	889	13 K
C2/m	200	1.39	700	67 K

As shown in Fig. 3d, at room temperature, two-step dimerization occurred at around 12 and 25 GPa, and P_4H_6 finally decomposed into elemental phosphorus at 35 GPa. However, at low temperature, P_2H_4 could exist up to 60 GPa. P_4H_6 was maintained from 102 to 205 GPa.

Theoretical calculations

We further performed structural searches on P_4H_6 at 100, 150 and 200 GPa with maximum simulation cells up to 4 formula units (f.u.); two stable structures with space group Cmcm (<182 GPa) and *C2/m* (>182 GPa) were found. Phonon dispersions calculations of the two structures do not give any imaginary frequencies and therefore this verifies their dynamic stabilities (Fig. 4). The superconducting T_c was estimated using the Allen and Dynes modified McMillan equation [34] with a typical choice of $\mu^* = 0.13$. The electron–phonon coupling constant λ of the Cmcm structure is only 0.59 (Table 1) at 100 GPa, and a superconducting T_c of 13 K was obtained. A relatively large λ value of 1.39 was found for the C2/m structure at 200 GPa, and the superconducting T_c was estimated to be 67 K. As summarized in Table 1, the estimated T_c agrees with the values measured by Drozdov *et al.*, suggesting that P_4H_6 could be responsible for the superconductivity.

Similar to H_2S, PH_3 is unstable at high pressure. Instead of becoming more hydrogen-enriching, it dehydrogenates through a series of polymerization/decomposition processes upon compression. This could be one of the critical factors that limit the maximum T_c near 100 K, at the same pressure where the H–S system has a T_c up to 180 K. These phenomena from H_2S and PH_3 highlight that avoiding the pressure-induced dehydrogenation or becoming more hydrogen-enriched is vital for a superconducting hydride with a high T_c.

CONCLUSION

In summary, we determined the stability of PH_3 under high pressure. At room temperature, two steps of polymerization were obtained. P_2H_4 and P_4H_6 were the reaction products of the first and second step

dimerization, respectively. Above 35 GPa, the generated P_4H_6 completely decomposed into elemental phosphorus. However, at low temperature, P_4H_6 could remain up to 205 GPa. Vibrational measurements and theoretical simulation confirmed the formation of P_2H_4 and P_4H_6, which enriches the phase diagram of the P–H system under high pressure. Our work proves that the P_4H_6 phase can be generated under high pressure and suggests that it might be responsible for the reported superconducting transition.

METHODS

Solidified PH_3 was prepared via a cryogenic method and sealed into a symmetric DAC at ∼2 GPa for our *in situ* high-pressure measurements. T301 stainless steel and tungsten gaskets were used for the room-temperature and low-temperature measurements, respectively. The ruby fluorescence and Raman shifts of the diamond were used to calibrate the pressure. A micro-Raman system (Renishaw, UK) with a 532-nm laser excitation was used to obtain the sample's Raman spectra. The high-pressure *in situ* IR spectra were collected on a Bruker VERTEX 70v FTIR spectrometer and a custom-built IR microscope. High-pressure XRD measurements were carried out at the BL15U1 beamline of the Shanghai Synchrotron Radiation Facility ($\lambda = 0.6199$ Å) [35]. Low temperature was generated by cryostat using liquid nitrogen. Detailed information about each cycle is provided in the Supplementary Materials, available as Supplementary Data at *NSR* online. The *ab initio* structure predictions for P_4H_6 were performed using the particle swarm optimization technique implemented in the CALYPSO code [36,37]. CALYPSO has been used to investigate many materials at high pressures [38–42]. The *ab initio* structure relaxations were performed using density functional theory with the Perdew–Burke–Ernzerhof generalized gradient approximation implemented in the Vienna *ab initio* simulation package (VASP) [43]. Details of the simulations are provided in the Supplementary Materials, available as Supplementary Data at *NSR* online.

SUPPLEMENTARY DATA

Supplementary data are available at *NSR* online.

FUNDING

This work was mainly supported by the National Natural Science Foundation of China (11874076), the National Science Associated Funding (NSAF, U1530402) and the Science Challenging Program (TZ2016001).

REFERENCES

1. Onnes HK. Disappearance of the electrical resistance of mercury at helium temperatures. *Proc K Ned Akad Wet* 1911; **14**: 113–5.
2. Onnes HK. The resistance of pure mercury at helium temperatures. *Commun Phys Lab Univ Leiden b* 1911; 120.
3. Ashcroft NW. Hydrogen dominant metallic alloys: high temperature superconductors? *Phys Rev Lett* 2004; **92**: 187002.
4. Eremets MI, Trojan IA and Medvedev SA *et al.* Superconductivity in hydrogen dominant materials: silane. *Science* 2008; **319**: 1506–9.
5. Gao G, Oganov AR and Bergara A *et al.* Superconducting high pressure phase of germane. *Phys Rev Lett* 2008; **101**: 107002.
6. Gao G, Wang H and Bergara A *et al.* Metallic and superconducting gallane under high pressure. *Phys Rev B* 2011; **84**: 064118.
7. Li Y, Gao G and Xie Y *et al.* Superconductivity at 100 K in dense $SiH_4(H_2)_2$ predicted by first principles. *Proc Natl Acad Sci USA* 2010; **107**: 15708–11.
8. Wang H, Tse JS and Tanaka K *et al.* Superconductive sodalite-like clathrate calcium hydride at high pressures. *Proc Natl Acad Sci USA* 2012; **109**: 6463–6.
9. Li Y, Hao J and Liu H *et al.* Pressure-stabilized superconductive yttrium hydrides. *Sci Rep* 2015; **5**: 9948.
10. Drozdov AP, Eremets MI and Troyan IA *et al.* Conventional superconductivity at 203 kelvin at high pressures in the sulfur hydride system. *Nature* 2015; **525**: 73–6.
11. Gao L, Xue YY and Chen F *et al.* Superconductivity up to 164 K in $HgBa_2Ca_{m-1}Cu_mO_{2m+2+\delta}$ (m=1, 2, and 3) under quasihydrostatic pressures. *Phys Rev B* 1994; **50**: 4260–3.
12. Duan D, Liu Y and Tian F *et al.* Pressure-induced metallization of dense $(H_2S)_2H_2$ with high-T_c superconductivity. *Sci Rep* 2015; **4**: 6968.
13. Li Y, Wang L and Liu H *et al.* Dissociation products and structures of solid H_2S at strong compression Yinwei. *Phys Rev B* 2016; **93**: 020103.
14. Einaga M, Sakata M and Ishikawa T *et al.* Crystal structure of the superconducting phase of sulfur hydride. *Nat Phys* 2016; **12**: 835–8.
15. Drozdov AP, Eremets MI and Troyan IA. Superconductivity above 100 K in PH_3 at high pressures. arXiv: 1508.06224.
16. Flores-Livas JA, Amsler M and Heil C *et al.* Superconductivity in metastable phases of phosphorus-hydride compounds under high pressure. *Phys Rev B* 2016; **93**: 020508.
17. Liu H, Li Y and Gao G *et al.* Crystal structure and superconductivity of PH_3 at high pressures. *J Phys Chem C* 2016; **120**: 3458–61.
18. Shamp A, Terpstra T and Bi T *et al.* Decomposition products of phosphine under pressure: PH_2 stable and superconducting? *J Am Chem Soc* 2016; **138**: 1884–92.
19. Bi T, Miller DP and Shamp A *et al.* Superconducting phases of phosphorus hydride under pressure: stabilization by mobile molecular hydrogen. *Angew Chem Int Ed* 2017; **129**: 10326–9.
20. Durajski AP. Quantitative analysis of nonadiabatic effects in dense H_3S and PH_3 superconductors. *Sci Rep* 2016; **6**: 38570.

21. Huang TH, Decius JC and Nibler JW. Raman and IR spectra of crystalline phosphine in the γ phase. *J Phys Chem Solids* 1977; **38**: 897–904.
22. Frankiss SG. Vibrational spectrum and structure of solid diphosphine. *Inorg Chem* 1968; **7**: 1931–3.
23. Odom JD, Wurrey CJ and Carreira LA *et al.* Vibrational spectra and structure of biphosphine and biphosphine-d4. *Inorg Chem* 1975; **14**: 2849–53.
24. Baudler M and Glinka K. Open-chain polyphosphorus hydrides (phosphines). *Chem Rev* 1994; **94**: 1273–97.
25. Olego DJ, Baumann JA and Schachter R. The microscope structures of amorphous phosphorus. *Solid State Commun* 1985; **53**: 905–8.
26. Winchester RAL, Whitby M and Shaffer MSP. Synthesis of pure phosphorus nanostructures. *Angew Chem Int Ed* 2009; **48**: 3616–21.
27. Nixon ER. The infrared spectrum of biphosphine. *J Phys Chem* 1956; **60**: 1054–9.
28. Frisch MJ, Trucks GW and Schlegel HB *et al.* Gaussian 09, revision A.02. *Gaussian Inc Wallingford CT* 2009; 34.
29. Mao N, Tang J and Xie L *et al.* Optical anisotropy of black phosphorus in the visible regime. *J Am Chem Soc* 2016; **138**: 300–5.
30. Sugai S and Shirotani I. Raman and infrared reflection spectroscopy in black phosphorus. *Solid State Commun* 1985; **53**: 753–5.
31. Wittig J and Matthias BT. Superconducting phosphorus. *Science* 1968; **160**: 994–5.
32. Kawamura H, Shirotani I and Tachikawa K. Anomalous superconductivity in black phosphorus under high pressures. *Solid State Commun* 1984; **49**: 879–81.
33. Karuzawa M, Ishizuka M and Endo S. The pressure effect on the superconducting transition temperature of black phosphorus. *J Phys Condens Matter* 2002; **14**: 10759–62.
34. Allen PB and Dynes RC. Transition temperature of strong-coupled superconductors reanalyzed. *Phys Rev B* 1975; **12**: 905–22.
35. Zhang LL, Yan S and Jiang S *et al.* Hard X-ray micro-focusing beamline at SSRF. *Nucl Sci Tech* 2015; **26**: 60101.
36. Wang Y, Lv J and Zhu L *et al.* Crystal structure prediction via particle-swarm optimization. *Phys Rev B* 2010; **82**: 1–8.
37. Wang Y, Lv J and Zhu L *et al.* CALYPSO: a method for crystal structure prediction. *Comput Phys Commun* 2012; **183**: 2063–70.
38. Li Y, Hao J and Liu H *et al.* The metallization and superconductivity of dense hydrogen sulfide. *J Chem Phys* 2014; **140**: 174712.
39. Lv J, Wang Y and Zhu L *et al.* Predicted novel high-pressure phases of lithium. *Phys Rev Lett* 2011; **106**: 015503.
40. Wang X, Wang Y and Miao M *et al.* Cagelike diamondoid nitrogen at high pressures. *Phys Rev Lett* 2012; **109**: 175502.
41. Errea I, Calandra M and Pickard CJ *et al.* Quantum hydrogen-bond symmetrization in the superconducting hydrogen sulfide system. *Nature* 2016; **532**: 81–4.
42. Peng F, Sun Y and Pickard CJ *et al.* Hydrogen clathrate structures in rare earth hydrides at high pressures: possible route to room-temperature superconductivity. *Phys Rev Lett* 2017; **119**: 107001.
43. Kresse G and Furthmüller J. Efficient iterative schemes for *ab initio* total-energy calculations using a plane-wave basis set. *Phys Rev B* 1996; **54**: 11169–86.